A Dual-Frequency DRA based MIMO Antenna System for Wireless Access Points

A Dual-Frequency DRA based MIMO Antenna System for Wireless Access Points

Journal:	*IET Microwaves, Antennas & Propagation*
Manuscript ID	MAP-2016-0671.R1
Manuscript Type:	Research Paper
Date Submitted by the Author:	02-Jan-2017
Complete List of Authors:	Sharawi, Mohammad; King Fahd University of Petroleum and Minerals (KFUPM), Electrical Engineering Podilchak, Symon; Heriot-Watt University, School of Engineering and Physical Sciences; Queen's University, Electrical and Computer Engineering Khan, Muhammmad; National University of Sciences and Technology, School of Electrical Engineering and Computer Science; King Fahd University of Petroleum & Minerals, Electrical Engineering Department Antar, Yahia; Royal Military College of Canada, Dept of Electrical & Computer Engineering
Keyword:	MIMO ANTENNAS, DIELECTRIC RESONATOR ANTENNAS, WIRELESS LAN, MULTIBAND ANTENNAS
Note: The following files were submitted by the author for peer review, but cannot be converted to PDF. You must view these files (e.g. movies) online.	
IET_MAP_Dual_Band_DRA_MIMO_Rev1.tex	

A Dual-Frequency DRA based MIMO Antenna System for Wireless Access Points

Mohammad S. Sharawi *, Symon K. Podilchak †, Muhammad U. Khan‡ and Yahia M. M. Antar §,

* Department of Electrical Engineering,King Fahd University of Petroleum and Minerals

Dhahran, 31261, Saudi Arabia, (email: *msharawi@kfupm.edu.sa*)

† Institute of Sensors, Signals and Systems within the School of Engineering and Physical Sciences at

Heriot-Watt University, Edinbrugh, UK, (email: *s.podilchak@hw.ac.uk*)

‡ School of Electrical Engineering & Computer Science (SEECS-NUST),H-12, Islamabad, Pakistan

(email: *umar.khan@seecs.edu.pk*)

§ Department of Electrical and Computer Engineering, Royal Military College, Kingston, ON, Canada (email:

antar-y@rmc.ca)

Abstract

An eight-element, dual-frequency, multiple-input-multiple-output (MIMO) antenna system is proposed. Cylindrical dielectric resonator antennas (cDRAs) were used as the radiating elements in the MIMO antenna system. One group of four cDRAs covers the 2.45 GHz band, while another four cover the second band at 5.8 GHz. A reflector element was also proposed to tilt the radiated beam patterns and reduce field correlations for the MIMO antenna system. The high band antenna elements were rotated 45° with respect to their low band counterparts, on the antenna ground plan, for compactness and PCB integration such that the complete antenna system occupies a volume of 160 mm by 160 mm by 14.8 mm. The measured bandwidths were at least 90 MHz and 200 MHz for the two bands of operation while the envelope correlation coefficient was less than 0.17. A study of different metallic reflectors was also provided in terms of the impedance matching, isolation, bandwidth and envelope correlation coefficient (ECC). Specific applications for the proposed design include wireless local area networks (WLANs) and other 4G access points.

Index Terms **- Dielectric Resonator Antennas, Wireless LAN, MIMO, Dual-Frequency.**

I. Introduction

Multiple-input-multiple-output (MIMO) technology is currently used in most wireless standards. It will be used in future technologies as well because of the advantages it provides in increasing the system throughput compared to single antenna/channel communications [1]. Current 802.11n wireless local area network (WLAN) standards employ MIMO technology and multiple antennas for wireless access points. These antenna configurations are generally visible in shops and buildings and typically occupy a large volume around the access point, and in some cases, almost twice the volume of the structure for the access point box [2]. More planar topologies are generally preferred and some multi-band MIMO antennas can also been found in the literature [3]-[8]. However, one major drawback with these types of multi-band metallic based printed MIMO antennas is their relatively low efficiency (not exceeding 65%) when using commercial substrates.

On the other hand, dielectric resonator antennas (DRAs) are known to offer high radiation efficiencies and ease of integration with other electronics when placed on a common substrate. Operation over a wide range of frequencies is possible by altering the size of the element or scaling the value of the employed dielectric constant. DRAs can also be designed for wide bandwidths or multi-band coverage and several multi-band and wideband/UWB DRA-based antennas have been proposed in literature such as those in [9]-[10]. These antennas use an involved probe feed, complicated fabrication processes, and require different material types making them expensive and complex to manufacture. Not to mention that the obtained efficiency at the various bands is not equal and the antennas can have difficulty with polarization purity.

Several other feeding mechanisms have been investigated in literature such as a microstrip-fed, aperture coupled slot beneath the DRA [11]-[12], and aperture coupling via a dielectric image guide in [13] and [14]. This later mechanism will yield lower losses at higher frequencies, but has a complex construction and is more costly than the conventional slot-coupled microstrip based method. Another approach that relied on straight forward microstrip-based feeding was considered in [15]. In particular, tapered microstrip feeds were proposed to provide field matching for DRAs with a low dielectric constant. This method provided good gain and a 75% improvement in the impedance bandwidth. When more commercial electronics are considered, designs with low complexity and reduced manufacturing costs are typically prefered. For instance, the slot coupled feeding method by microstrip excitation is very attractive for such electronic system applications. This is because it is planar and compatible with printed circuit board (PCB) technology. Also, since the DRAs will be placed on a ground plane in these configurations and fed by microstrip using an aperture coupled slot, reduced coupling can be expected with other electronic components placed on the microstrip layer.

The use of DRA-based MIMO antennas with simple feeding has not been widely investigated in the literature and additional antenna research should be encouraged to achieve improved MIMO system performance. A few works have been reported

addressing these issues such as those in [16]-[20]. For example, a multi-band DRA-based MIMO antenna system covering 790 to 862 MHz, 2.45 GHz and 3.5 GHz was proposed in [16]. The dielectric constant of the rectangular dielectric resonator antennas (rDRAs), in the two-element MIMO configuration, was 37. A z-shaped microstrip feed line was used to excite the different modes and the two-element DRA-based MIMO antennas were placed within very few millimeters from each other achieving an envelope correlation coefficient of less than 0.42 in all bands. In [17] a six-port DRA-based array was also investigated. The array consisted of two rDRAs each with three-ports to have a six-port MIMO antenna structure. The array operated in the 2.6 GHz band and used a dielectric constant of 19.6. In [18] a reconfigurable DRA-based MIMO antenna was implemented where active diodes were utilized to achieve multi-band operation. The antenna covered bands between 630 to 790 MHz and utilized a half-cylindrical DRA with ϵ_r = 18. Following these developments, a single DRA with two probe feeds to obtain polarization diversity for a 2×2 MIMO antenna system was proposed in [19]. However, operation was demonstrated at a single band. Another rDRA structure was proposed in [20] where three excitation points were employed using an individual element to resemble a three-element MIMO antenna system. It should be mentioned that in all these works the feeding mechanism was non-planar. Moreover, probe location and proper placement required very high precision to excite the desired modes for radiation. It should also be mentioned that antenna efficiency and field coupling can be problematic with these designs, especially during simultaneous multiplexing operation, since multiple probes excite a single DRA element.

In this work a dual-frequency, 4-element MIMO antenna system is proposed with a simple feeding mechanism which can be operated in a 4×4 MIMO configuration within each of the two bands covered in wireless access point applications. To achieve optimal antenna efficiency, high throughput and low field coupling (good polarization performance), four cylindrical dielectric resonator antenna (cDRA) elements were developed for each band to yield a 4-element MIMO antenna system. More specifically, the two bands covered are the 2.45 and 5.8 GHz WLAN bands with at least 100 MHz of bandwidth in each. The two MIMO antenna systems were rotated by 45° with respect to each other to occupy the smallest area on the ground plane as discussed in Section II. A center metallic reflector element to reduce the correlation coefficients via tilting the fields and thus improving the system operation is introduced. The effect of this metallic center reflector on the isolation, bandwidth, radiation and correlation of the MIMO antenna system is also investigated in Section III. Practical fabrication considerations such as the effect of the bonding agent and the slot alignment are discussed in details for the first time showing their effect on the performance of cDRAs. The overall system size is 160 mm by 160 mm by 14.8 mm and simulation and measurement results are in agreement. The worst case correlation coefficient value obtained was 0.167 in both bands. It should be mentioned that this paper builds on the earlier findings in [21] where some preliminary findings were presented. More importantly, the designed, fabricated, and measured MIMO antenna system reported in this paper (which follows [21]) including all the details

and analysis of various practical effects offers a much smaller volume (low profile) when compared to currently deployed and commercially available wireless access point systems that enable 4G communications [22]-[23].

II. Dual-Frequency DRA MIMO Design

The configuration of the proposed low-profile, dual-frequency, cDRA-based MIMO antenna system is shown in Fig. 1(a),(b). The antenna system consists of four antennas covering the 2.45 GHz WLAN band (labeled DRAs 1 to 4) and another four antennas covering the 5.8 GHz band (labeled DRAs 5 to 8) for excitation of the $HEM_{11+\delta}$ and $TE_{01+\delta}$ modes, respectively. The diameter and height of DRAs 1 to 4 are 25.4 mm and $h1$ = 14 mm, while for DRAs 5 through 8, the diameter and height are 15.9 mm and $h2$ = 5 mm, respectively. Both DRA types were machined from HiK500 material with ϵ_r = 10 and $tan\ \delta$ = 0.002. The four lower band antennas were placed at 90° angles along a circle with radius 55 mm ($D1$ = 25 mm), while the higher band antennas were placed on a circle of radius 30 mm (thus $D2$ = 12.05 mm, assuming a center reflector diameter of 20 mm) and rotated 45° with respect to the larger DRA elements. The two center reflector (Cylindrical and Cross Shaped) types investigated in this work are shown in the inset of the figure. The cDRA element sizes for the lower and higher bands were initially determined using [12]:

$$f = \frac{30k_0a}{2\pi h\frac{a}{h}} \tag{1}$$

where f is the resonant frequency of the mode in GHz, k_0 is the wavenumber in free space, a and h is the radius and height of the cDRA in cm, respectively. For each excited mode, the geometry, material and size of the cDRA will determine its resonance frequency, the bandwidth of operation, and the quality factor. For $HEM_{11+\delta}$ mode excitation and $0.4 \leq \left(\frac{a}{h}\right) \leq 6.0$ [24], [25]:

$$k_0a = \frac{6.324}{\sqrt{\epsilon_r+2}}\left(0.27 + 0.36\left(\frac{a}{2h}\right) - 0.02\left(\frac{a}{2h}\right)^2\right) \tag{2}$$

$$Q = 0.01007\epsilon_r^{1.3}\frac{a}{h}\left(1 + 100e^{-2.05\left(\frac{a}{2h} - \frac{1}{80}\left(\frac{1}{h}^2\right)\right)}\right) \tag{3}$$

where Q is the quality factor of the mode excited. For a $TE_{01+\delta}$ mode with $0.33 \leq \left(\frac{a}{h}\right) \leq 5.0$,

$$k_0a = \frac{2.327}{\sqrt{\epsilon_r+1}}\left(1 + 0.2123\left(\frac{a}{h}\right) - 0.00898\left(\frac{a}{h}\right)^2\right) \tag{4}$$

$$Q = 0.078192\epsilon_r^{1.27}\left(1 + 17.31\left(\frac{h}{a}\right) - 21.57\left(\frac{h}{a}\right)^2 + 10.86\left(\frac{h}{a}\right)^3 - 1.98\left(\frac{h}{a}\right)^4\right). \tag{5}$$

Both antenna types were excited via a slot coupling mechanism. The feed network consisted of 50-Ω microstrip transmission lines on the bottom layer of the board, and the coupling slots for each DRA was centered beneath. The lower band DRAs had

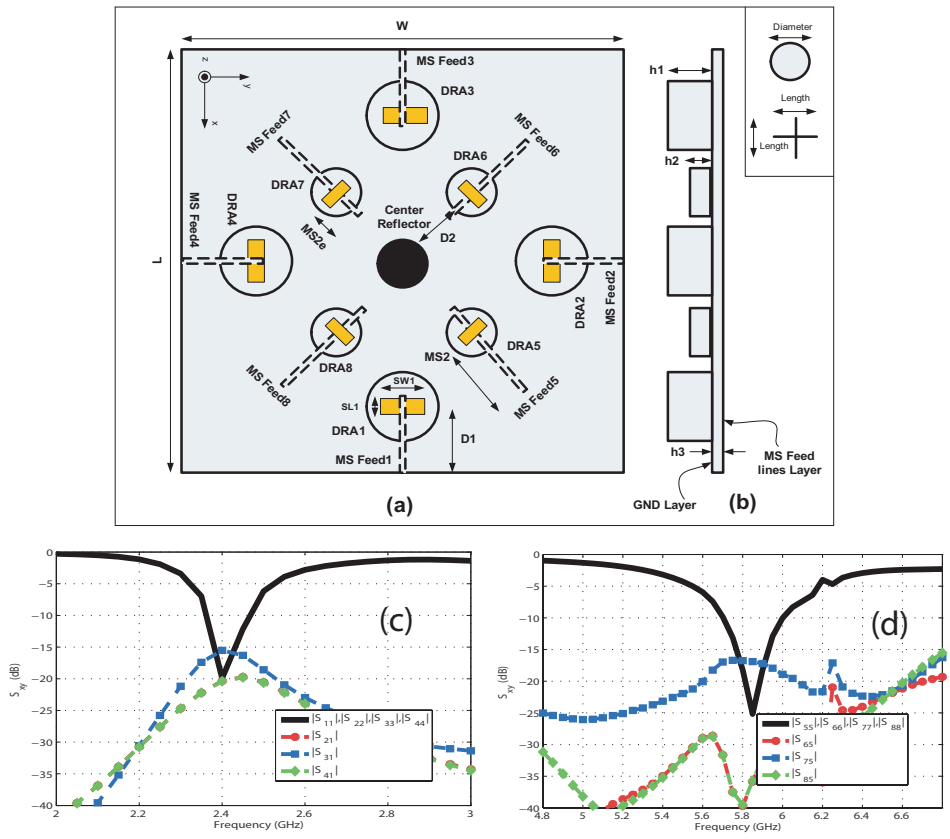

Fig. 1. Diagram of the cDRA dual-frequency MIMO antenna system: (a) the top view and (b) the side view. Dashed lines are on the bottom layer, and slots are on the top ground plane layer (all dimensions are in mm), (c) Simulated S-parameter curves for low band elements, (d) Simulated S-parameter curves for the higher band.

slot dimensions of 11 mm by 16 mm with the feed line extended 3 mm beyond its center for impedance matching, and the higher band DRAs had slot dimensions of 8 mm by 9 mm, with the feed line extended by 9 mm beyond its center. It is very important to have good coupling between the excitation slot and the cDRA, as any coupling degradation will affect the final operating bandwidth of the cDRA via the change of its original Q-factor to the loaded Q-factor (Q_L).

The slot location and size should be optimized to ensure high coupling from the feeding transmission line to the cDRA. The effect of a center metallic reflector was also investigated with diameters not exceeding 30 mm and heights not exceeding 40 mm. The complete antenna system is built on a two layer RO3003 substrate with ϵ_r = 3, $tan\delta$ = 0.001, and 160 mm by 160 mm by 0.762 mm in size. SMA connectors were also used as feeding ports to the antenna system.

III. Antenna Operation and Practical Considerations

The dual-frequency MIMO antenna system was modeled and optimized using HFSS^{TM}. The simulated reflection coefficient and port isolation values for the proposed design are shown in Fig. 1(c),(d) for both the lower and higher bands, respectively. It is clear that the low-band antennas resonate at 2.4 GHz with a minimum -10 dB bandwidth of 100 MHz. It should be

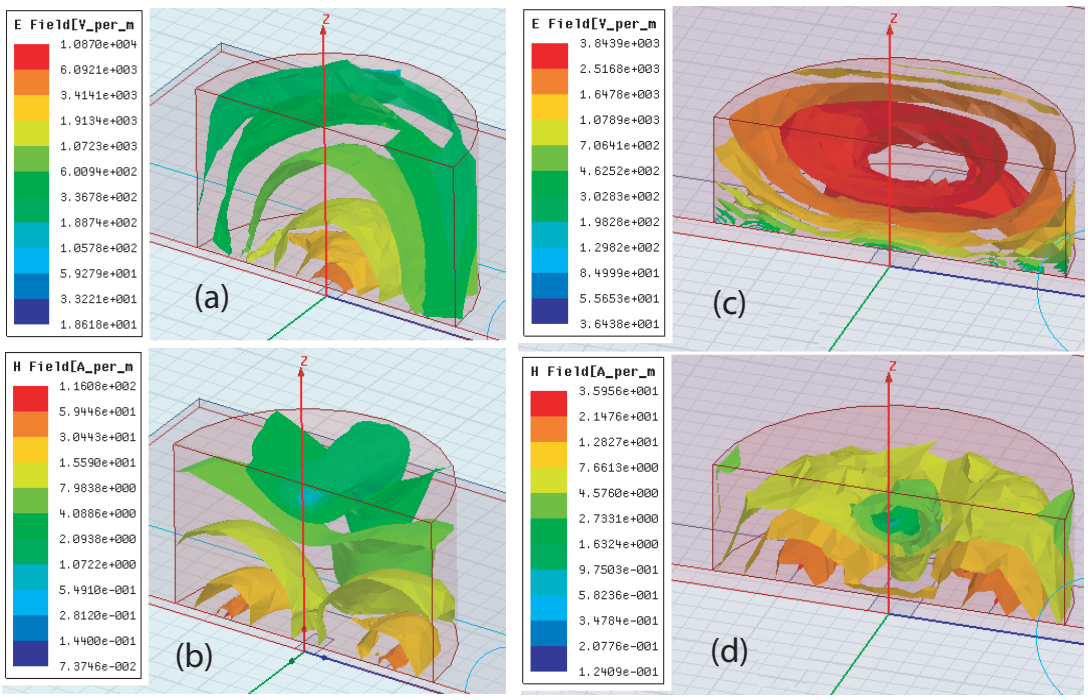

Fig. 2. DRA internally excited fields, (a) E-field lower band, (b) H-filed higher band, (c) E-field lower band and (d) H-field higher band.

mentioned that the calculated values from (1)-(3) give resonances at 2.78 and 5.54 GHz for the two bands, respectively. Note that these equations do not take into account the coupling or finite ground plane effects and thus some minor adjustments to the DRA dimensions was required. It can also be observed that the isolation between the lower band elements is always greater than 15 dB across the band of operation. For the higher band cDRAs, the center frequency was around 5.8 GHz with an operating bandwidth of at least 300 MHz and isolation levels better than 17 dB.

The simulated fields inside the cDRAs are shown in Fig. 2 (a),(b) and (c),(d) for the lower band and higher band DRAs electric (E) and magnetic (H) fields, respectively. The E and H fields for the lower operating frequency band for DRAs 1 to 4 in Fig. 2 (a),(b) illustrate modes of the $HEM_{11\delta}$ kind, while those in Fig. 2 (c),(d) for the higher band of operation (DRAs 5 to 8), show $TE_{01\delta}$ mode excitation.

Fig. 3(a) shows the top view of the array (DRA side) of the fabricated prototype with two feeding slots exposed (DRAs A1 and A6 removed), and Fig. 3(b) shows the bottom side (feed network) before attaching the connectors along with the mounting fixture. The measurement setup is shown in Fig.3 (c),(d). It should be noted that the fabricated cDRAs were machined with highest accuracy, and the obtained heights were 13.98, 13.98, 14.0, and 14.02 mm, and 5.03, 5.02, 5.02, and 5.03 mm for the low and high band DRAs, respectively. The DRAs were then glued onto the ground plane using a bonding material with ϵ_r = 3.3 with a thickness of approximately 100μm. Thus, for accurate comparison between simulations and measurements, the effect of the bonding agent thickness as well as the coupling slot placement shifts were investigated via simulations to assess

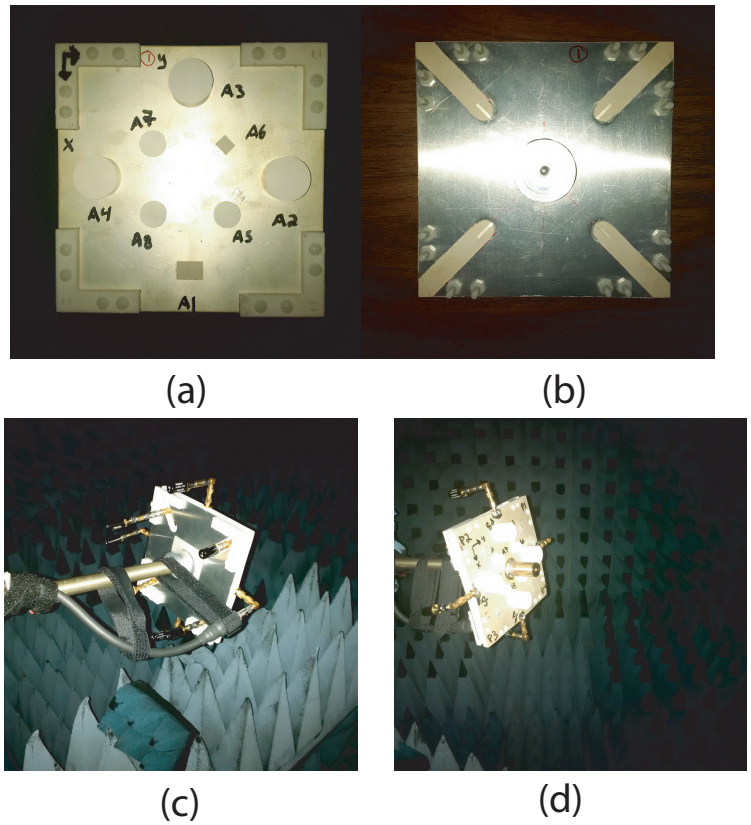

Fig. 3. Fabricated dual-frequency cDRA MIMO antenna, (a)top view (DRA and ground plane side), (b) bottom view (feed network side), (c) measurement setup with terminators, and (d) large reflector mounted on the antena system.

their effects on the frequency response of the various cDRAs.

1) Bonding Agent Thickness: The effect of the thickness of the employed boding agent (ϵ_r = 3.3, with loss tangent of approximately 0.002) on the minimum of the reflection coefficient was examined. In particular, simulations for the reflection coefficient curves are shown in Fig. 4(a),(b) when the bonding agent thickness was varied from 50 μm up to 300 μm (in 50 μm steps) for the lower and upper bands, respectively. All other parameters were kept constant for the original design model as described earlier. It is clear that the bonding agent can shift the resonance frequency of various DRAs by as high as 100 MHz.

2) DRA Position with Relation to the Microstrip-Fed Slots: The effect of DRA misalignment on the reflection coefficients for the DRAs in both bands was also investigated because the cDRAs were manually placed using a microscope with accuracies +/- 0.4 mm. Fig. 4(c) and (d) shows the various curves where the DRA position was varied between -0.6 to 0.6 mm in the vertical direction (x while y is fixed) for the low and high bands, respectively. More specifically, Fig. 4(c) shows the effect of different DRA placements along the x-axis (DRA-1 is shown, but similar behaviour was obtained for other DRAs), while Fig. 4(d) shows the effect of such shifts in the higher band. It can be observed that minor variations in the DRA placement from the ideal can yield a slight shift in the reflection coefficient minimum, and that a worst case shift of about 50 MHz is

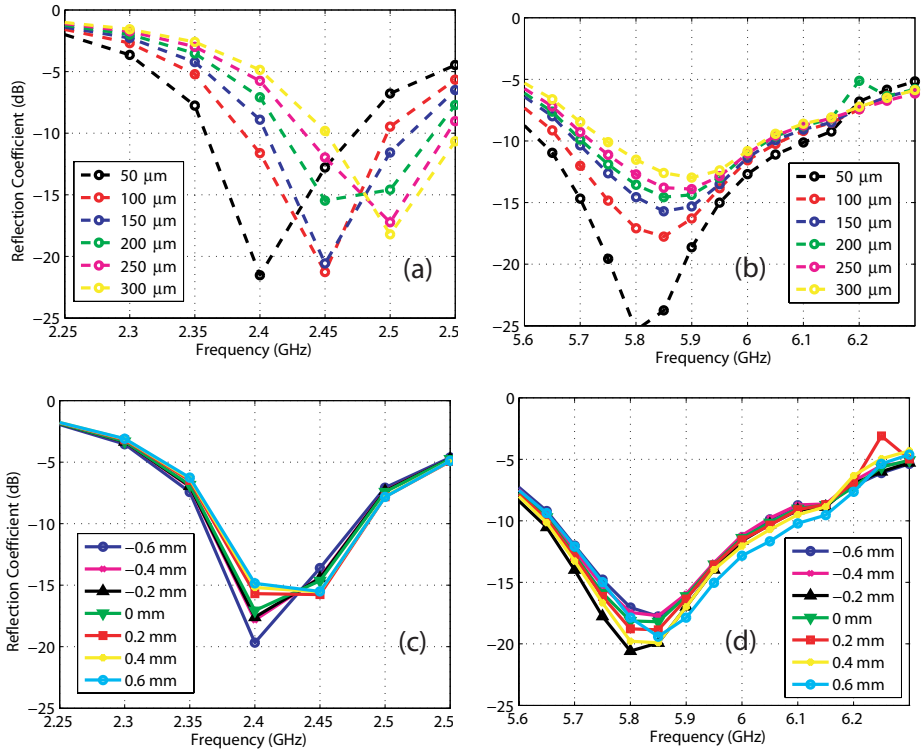

Fig. 4. Simulated fabrication variations, (a) effect of boding agent thickness at lower band, (b) effect of bonding agent thickness at higher band, (c) effect of slot coupling shift in lower band and (d) effect of slot coupling shift in higher band.

possible in frequency for both the upper and lower band elements. Similar behaviour was observed when fixing x and varying y coupling slot positions.

IV. Prototype results, MIMO Operation and Reflector effects

A. *Port parameters*

The measured lower and higher band reflection coefficient curves are shown along with the simulated ones in Fig. 5(a) and (b), for the lower and higher bands, respectively. Also, the port isolation curves are presented in Fig. 5.(c), (d). A minimum measured bandwidth of 90 MHz is obtained in the lower band and 200 MHz in the higher band with an isolation of at least 16 dB. This means that there is no need to use complex and costly isolation enhancement strucutres. Results are in agreement and it should be mentioned that all these measurements and simulations were completed without the placement of the center reflector. However, some shifts in the center frequencies of the reflection coefficients for the measurements can be observed when compared to the simulations. This can be attributed to the use of the bonding material, DRA placement over the coupling slots, as well as the slight differences in the fabricated DRA heights.

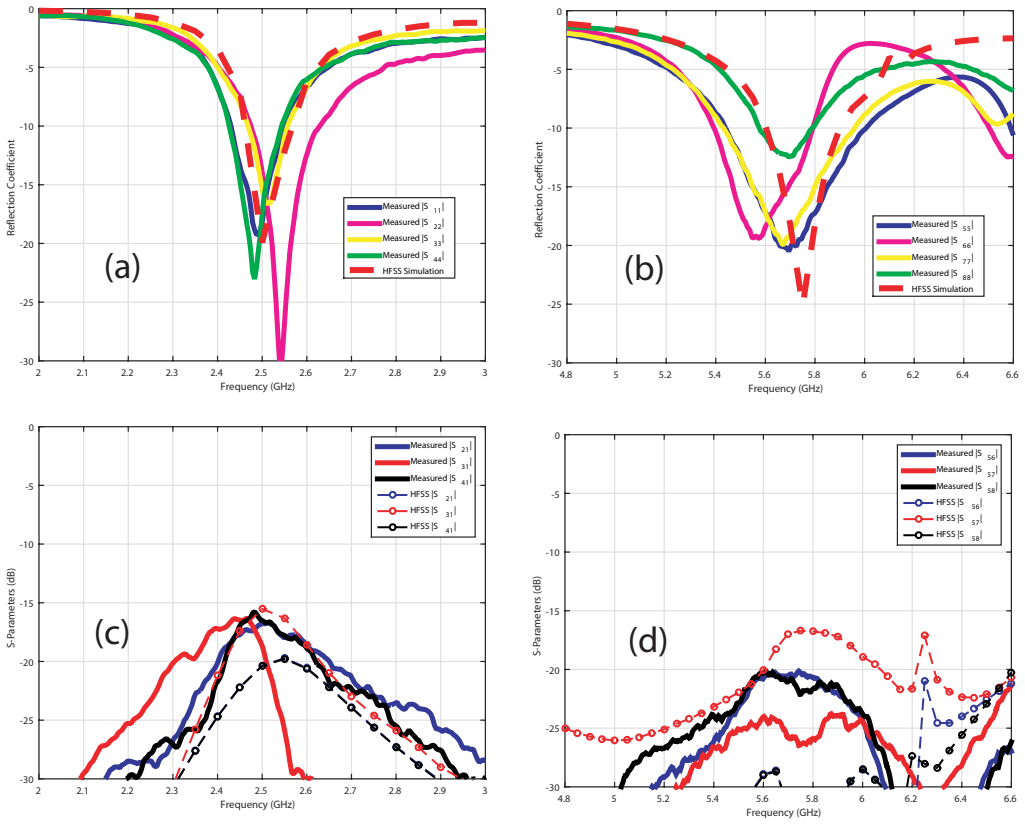

Fig. 5. Measured and simulated S-parameters of the individual elements, (a) lower band S_{xx}, (b) higher band S_{xx}, (c) lower band S_{xy}, (d) higher band S_{xy}.

B. Beam Tilting and MIMO Performance Evaluation

The simulated radiation efficiency of the lower band elements was 97%, while for the higher band elements it was 98%. The obtained maximum gain values for the individual elements were about 6.5 dBi and 8.9 dBi for all antennas at 2.45 GHz and 5.8 GHz, respectively. The envelope correlation coefficient (ECC) or ρ_e, and the correlation coefficient (ρ), are important parameters that need to be evaluated for the antenna system to ensure proper MIMO functionality. These metrics define the independence of the communication channels in a MIMO system configuration, and thus play a major role to enhance data throughput from multiple un-correlated channels. The ECC values between various elements within the same band were calculated based on their 3D radiation patterns and using the field equation [2],

$$\rho_e = ECC = \frac{\left| \iint_0^{4\pi} \left[\vec{F}_1(\theta,\phi) * \vec{F}_2(\theta,\phi) \right] d\Omega \right|^2}{\iint_0^{4\pi} \left| \vec{F}_1(\theta,\phi) \right|^2 d\Omega \iint_0^{4\pi} \left| \vec{F}_2(\theta,\phi) \right|^2 d\Omega} \tag{6}$$

where $\vec{F}_i(\theta,\phi)$ is the 3D complex field pattern of antenna element i. The complex total radiated fields were used in the calculation and the envelope correlation coefficient (ECC) values between the lower band elements did not exceed 0.167 while

the ECC values for the higher band did not exceed 0.0547. This is a good indication that the proposed MIMO antenna system satisfies the 0.3 maximum correlation coefficient (0.5 for ECC) value set by the standard [2].

The ECC was evaluated using the simulated 3D field patterns at the center frequencies of the two covered bands as well as the two frequency points where $|S_{11}|$ = -10 dB[1] and compared against the values computed using the measured port parameters for the four elements within the lower and higher bands. This comparison is important since DRAs can be considered as efficient radiators, and as such, a comparison between the far-field computed ECC and the ECC obtained from the measured S-parameters is of value. In particular, Fig. 6(a) shows the ECC values at the lower band, while Fig. 6(b) reports the ECC values for the higher band. In both bands, the ECC values calculated using the 3D complex field patterns agreed well with the ones obtained by the S-parameters. This important observation stresses the fact that the S-parameter method is not as accurate for ECC calculations since it ignores the shapes of the tilted patterns even for highly efficient antennas such as cDRAs. Regardless of this fact, the ECC values obtained in both bands did not exceed 0.17 indicating good MIMO operation and suggesting diversity behavior for the proposed antenna system.

C. Considerations for the Center Reflector

Different sizes of a center metallic reflector were also examined to understand the effects on antenna resonance, achievable bandwidths, isolation between the elements and directive patterns. More specifically, two types of center reflectors were examined; a cylindrical solid reflector, and a cross-shaped sheet (thin) reflector. Several reflector sizes from each type were examined and results are summarized in Tables I to IV. ECC values were also tabulated using the 3D complex field patterns of the antennas. It should also be mentioned that the first row in each of the tables with a very small reflector height (0.1mm), is representative of the no reflector cases.

Tables I and II show the effect of the cylindrical shaped reflector for the MIMO antenna system at the 2.4 GHz lower band and the 5.8 GHz higher one, respectively. The best input impedance matching (lowest reflection coefficient magnitude) and widest bandwidth (BW) occurs without the presence of the center reflector. However, the general trend can be observed that increased port isolation can be obtained between adjacent elements when using this metallic object. This improved isolation is evident regardless of the reflector size in the lower band, while for the higher band, only a couple of cases show less isolation improvement.

[1]The simulated 3D field patterns were used to evaluate the ECC values because the far-field measurement setup could only provide a limited number angular plane cuts. This was not sufficient to evaluate the ECC since full 3D patterns are required as outlined by Eq. (6). However, since good agreement was obtained between the 2D simulated and the measured beam patterns (see Fig. 7), we have confidence that the ECC values obtained from the simulated fields can provide a suitable representation.

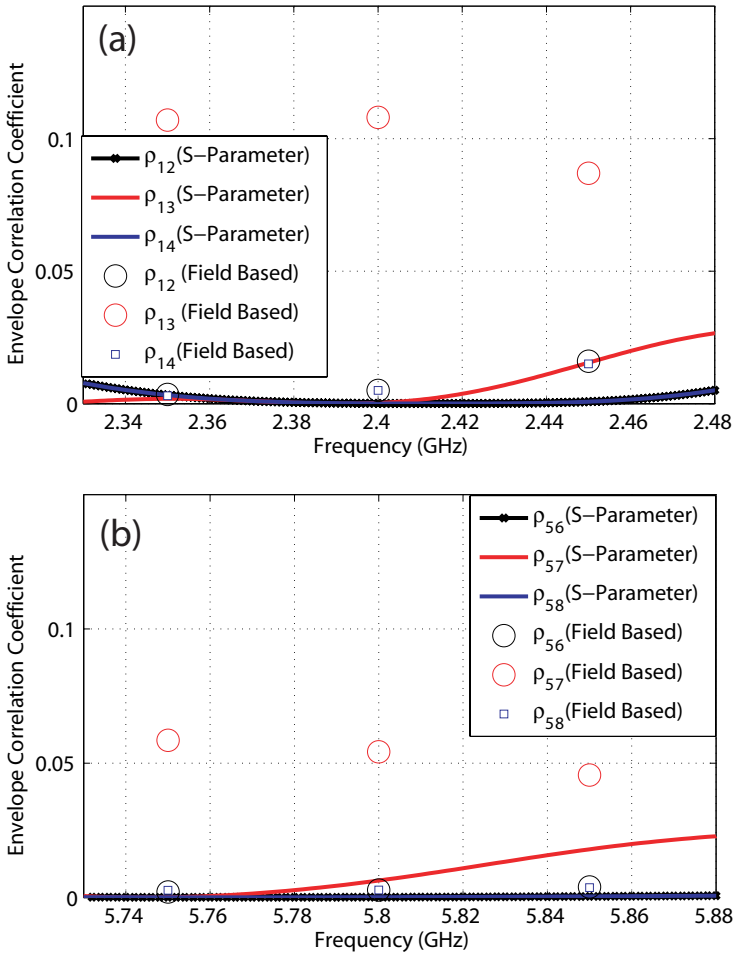

Fig. 6. ECC values using 3D simulated fields and measured S-parameters, (a) lower band (2.4 GHz), (b) higher band (5.8 GHz).

It should also be mentioned that the center reflector size can slightly enhance pattern directivity when using larger sizes (by almost 1 dB) at the higher bands, but at a cost of lower impedance matching and bandwidth. As observed in Tables III and IV, when using the cross-shaped reflector, a better performance can be obtained when using thin and tall sheets compared to the no reflector case, where good matching as well as isolation and bandwidth can be obtained when using a 20 and 40 mm sheet length and height, respectively. In addition, the larger the reflector the higher the directivity. But care should also be taken, that once the reflector starts getting closer to the DRA elements, degradation in antenna efficiency and matching is possible.

The effect of the small and large reflectors on the ECC calculations also showed some improvement. As outlined in the previous section beam tilting will yield improved ECC performance. This was also confirmed by the ECC calculations using Eq. (6). For example, without a center reflector, the worst case ECC at the lower bands was 0.167, while using the large cylindrical reflector it went down to 0.037. This is possible because the larger reflectors can further tilt the beams enhancing directivity. This will come at the cost of a higher profile if larger reflectors are targeted. This will also give better ECC than

TABLE I

CENTER CYLINDRICAL REFLECTOR EFFECTS (LOW BAND).

Diameter	Height	f_c	$\|S_{11}\|$	Min Isolation	BW	Max ECC
(mm)	(mm)	(GHz)	(dB)	(dB)	(MHz)	$\times 10^{-2}$
20	0.1	2.4	-22	15	100	16.7
20	14	2.4	-18	15.5	100	9.4
20	28	2.4	-15.5	19.6	70	8.5
20	40	2.4	-19	17	85	4.28
30	14	2.4	-16	16	90	10.1
30	28	2.4	-16	19.7	80	9.2
30	40	2.4	-14.5	19.6	55	3.7

TABLE II

CENTER CYLINDRICAL REFLECTOR EFFECTS (HIGH BAND).

Diameter	Height	f_c	$\|S_{11}\|$	Min Isolation	BW	Max ECC
(mm)	(mm)	(GHz)	(dB)	(dB)	(MHz)	$\times 10^{-2}$
20	0.1	5.8	-27	18	400	5.47
20	14	5.85	-17	16	280	2.59
20	28	5.75	-19	21.6	300	0.46
20	40	5.8	-23	21	350	0.35
30	14	5.9	-13	13	260	2.24
30	28	5.85	-15	19	250	0.29
30	40	5.95	-16.7	18.5	290	0.18

using the conventional monopoles that have omnidirectional radiation patterns as in current access point designs. The tables show that the cylindrical reflector can provide better ECC at the lower bands.

Two prototypes incorporating a cylindrical center reflector with diameter of 20 mm, and heights of 14 mm and 40 mm were fabricated. Fig. 3(d) shows the prototype with the cylindrical reflector attached to its center. The smaller reflector (14 mm height) had a minimum measured bandwidth of 90 MHz at the 2.45 GHz band, and a maximum bandwidth of 210 MHz. The minimum measured isolation in this band was 12.5 dB. For the 5.8 GHz band, the minimum measured bandwidth was 200 MHz, while the maximum was 387 MHz. The minimum isolation was 18 dB. Using the larger reflector (40 mm height), the lower band minimum measured bandwidth was 90 MHz, while the maximum was 131 MHz. The minimum measured isolation

TABLE III

CENTER CROSS-SHAPED REFLECTOR EFFECTS (LOW BAND).

Length	Height	f_c	$\|S_{11}\|$	Min Isolation	BW	Max ECC
(mm)	(mm)	(GHz)	(dB)	(dB)	(MHz)	$\times 10^{-2}$
20	0.1	2.4	-22	15	100	16.7
20	14	2.4	-19	14	110	14.4
20	28	2.4	-17.4	16	130	13.6
20	40	2.4	-30	16	90	12
30	14	2.4	-18	14	110	15.2
30	28	2.4	-16	15	78	14.6
30	40	2.4	-22	17	90	11.9

TABLE IV

CENTER CROSS-SHAPED REFLECTOR EFFECTS (HIGH BAND).

Length	Height	f_c	$\|S_{11}\|$	Min Isolation	BW	Max ECC
(mm)	(mm)	(GHz)	(dB)	(dB)	(MHz)	$\times 10^{-2}$
20	0.1	5.8	-27	18	400	5.46
20	14	5.77	-23	17	350	1.84
20	28	5.75	-22	20	310	0.24
20	40	5.75	-30	21	350	0.24
30	14	5.8	-13	12.6	210	2.73
30	28	5.75	-16	23.3	270	0.17
30	40	5.77	-24	21	340	0.03

was 14 dB. For the higher band, the minimum measured bandwidth was 240 MHz, while the maximum was 560 MHz, with minimum isolation of 24 dB. These values are in agreement with Table I to IV.

These findings and the results in Tables I through IV can serve as a starting point to help the MIMO antenna system designer understand the design tradeoffs when using such reflectors in terms of bandwidth, isolation, matching and beam-tilts/ECC performance. In the next section measured far-field patterns are reported and results are compared to the simulations using a commercial full-wave solver.

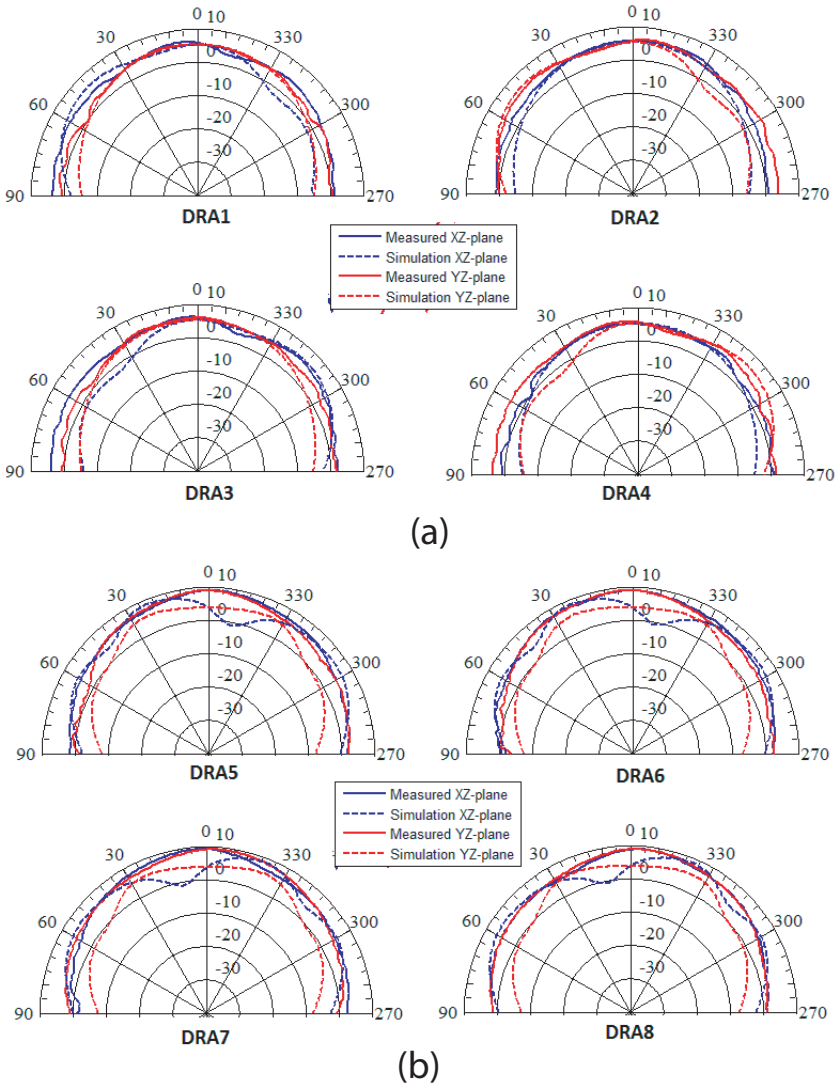

Fig. 7. Measured and simulated 2D gain patterns for the no-reflector cases, (a) DRA1-DRA4 and (b) DRA5-DRA8.

D. Radiation Pattern Measurements

The MIMO antenna system was measured in a far-field anechoic chamber and the 2D gain patterns were recorded for the upper half sphere. Pictures of the setup are shown in Fig. 3(c) and (d). A dual-ridge horn antenna (ETS-3115) was used for chamber calibrations and had a gain of 8.5 dB at 2.4 GHz and 11.5 dB at 5.8 GHz. The simulated and measured co-pol gain patterns for the principle planes (xz, yz) for both center frequency bands are shown in Fig. 7 for all antenna elements. The measured patterns for cDRA 5-8 were conducted at 45° angles in azimuth; i.e. the elevation cuts were made at 45°, 135°, 225° and 315° in azimuth for DRAs 5-8, respectively, and thus were made on their axis of maximum radiation. A maximum gain of approximately 4.5 dBi was obtained for cDRAs 1 to 4 and 9.5 dBi for cDRAs 5 to 8 which is in agreement with the simulations. Good agreement is observed with some slight beam broadening in the measured pattern.

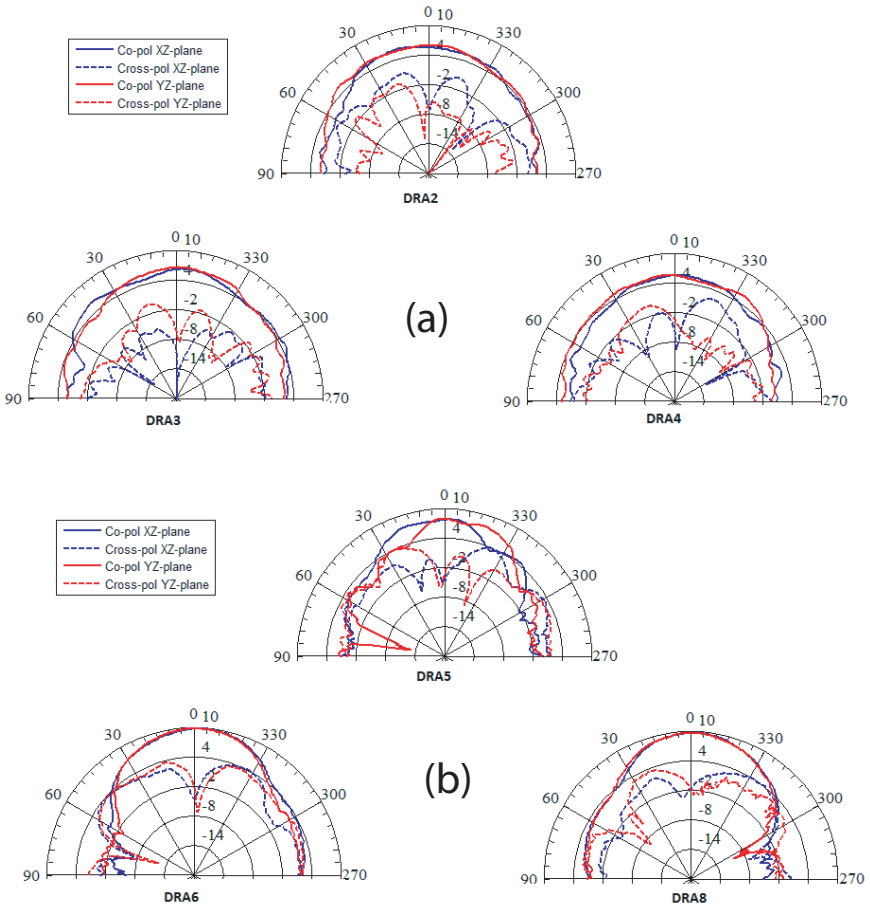

Fig. 8. Measured 2D gain patterns (co-pol and cross-pol) for the large-reflector cases, (a) lower band, (b) higher band.

Fig. 8 shows the gain patterns when the large cylindrical reflector was attached to the middle of the MIMO antenna system ground plane. Clearer tilts in the beam patterns and narrower beam widths (i.e. higher directivity) can be observed at the higher frequency band (i.e. cDRA 5, 6 and 8) with slightly higher gain and narrower beam width when compared to the no reflector case ($\sim 5-8^{\circ}$ in the direction of beam maximum is observed). This configuration will provide good MIMO performance and lower channel correlation because of the minimal antenna coupling and field correlation. For indoor access point applications, such radiation patterns are acceptable because of the nature of the rich multipath environment that will allow the signals to come from various directions and thus pure horizontal coverage is not required, not to mention that the placement of the access point at a higher position than the user will relax any condition of having larger horizontal coverage. This is inline with the patterns provided in [3], [4] and [17].

V. Conclusions

A low-profile, dual-frequency, DRA-Based MIMO antenna system for wireless access points was presented. The design had four antenna elements for each of the two bands defining a 4×4 MIMO systems for high data throughput and channel capacity.

The WLAN bands of 2.45 GHz and 5.8 GHz were covered. Wide operating bandwidths with high efficiency and low isolation were achieved. The overall size of the proposed MIMO antenna system was 160 mm by 160 mm by 14.8 mm. A detailed discussion regarding the fabrication and assembly process was also included. The benefits of attaching different center metallic reflectors was also demonstrated. These relatively small reflectors will not complicate the design procedure or increase antenna profile. More importantly, these relatively simple, and novel, center reflectors can improve element isolation and directivity (especially on the higher band operation), while also causing minimal affects to the efficiency of MIMO antenna, the bandwidth of operation, and impedance matching.

ACKNOWLEDGEMENTS

The authors would like to acknowledge the support provided by the Deanship of Scientific Research (DSR) at King Fahd University of Petroleum and Minerals (KFUPM), Dhahran, Saudi Arabia, under project number RG-1419.

REFERENCES

[1] M. A. Jensen and J. W. Wallace, "A Review of Antennas and Propagation for MIMO Wireless Communications," *IEEE Transactions on Antennas and Propagation*, Vol. 52, No. 11, pp. 2810-2824, November 2004.

[2] M. S. Sharawi, *Printed MIMO Antenna Engineering*, Artech House, 2014.

[3] S.W. Su, "High-Gain Dual-Loop Antennas for MIMO Access Points in the 2.4/5.2/5.8 GHz Bands," *IEEE Transactions on Antennas and Propagation*, Vol. 58, No. 7, pp. 2412-2419, Jul. 2010.

[4] S.-W. Su, "Very Low Profile Monopole antennas for Concurrent 2.4-5 GHz WLAN Access Point Applications," *Microwave and Optical Technology Letters*, Vol. 51, No.11, pp. 2614-2617, 2009.

[5] X. M. Ling and R. L. Li, 'A Novel Dual-Band MIMO Antenna Array With Low Mutual Coupling for Portable Wireless Devices," *IEEE Antennas and Wireless Propagation Letters*, Vol. 10, pp. 1039-1042, 2011.

[6] M. S. Sharawi, A. B. Numan, M. U. Khan, and D. N. Aloi, "A Dual-Element Dual-Band MIMO Antenna System with Enhanced Isolation for Mobile Terminals," *IEEE Antennas and Wireless Propagation Letters*, Vol. 11, pp. 1006-1009, 2012.

[7] S.C. Fernadnez and S.K. Sharma, "Multiband Printed Meandered Loop Antennas with MIMO Implementations for Wireless Routers," *IEEE Antennas and Wireless Propagation Letters*, Vol. 12, pp. 96-99, 2013.

[8] R. Karimian, H. Oraizi, S. Fakhte, and M. Farahani, "Novel F-Shaped Quad-Band Printed Slot Antenna for WLAN and WiMAX MIMO Systems," *IEEE Antennas and Wireless Propagation Letters*, Vol. 12, pp. 405-408, 2013.

[9] K. K. So and K. W. Leung, "Bandwidth Enhancement and Frequency Tuning of the Dielectric Resonator Antenna Using a Parasitic Slot in the Ground Plane", *IEEE Transactions on Antennas and Propagation*, Vol. 53, No. 12, pp. 4169-4172, December 2005.

[10] Yong-Xin Guo, Yu-Feng Ruan, and Xiang-Quan Shi, "Wide-Band Stacked Double Annular-Ring Dielectric Resonator Antenna at the End-Fire Mode Operation", *IEEE Transactions on Antennas and Propagation*, Vol. 53, No. 10, pp. 3394-3397, October 2005.

[11] J.T.H. St-Martin, Y.M.M. Antar, A.A. Kishk, A. Ittipiboon and M. Cuhaci, "Dielectric Resonator Antenna Using Aperture Coupling", *Electronics Letters*, Vol. 26, No. 24, pp. 2015-2016, December 1990.

[12] R. K. Mongia and P Bhartia, "Dielectric Resonator Antennas A Review and General Design Relations for Resonant Frequency and Bandwidth," International Journal on RF and Microwave Computer Aided Engineering, Vol. 4, No. 3, pp. 230-247, July 1994.

[13] A. S. Al-Zoubi, A. A. Kishk and A. W. Glisson, "Aperture Coupled Rectangular Dielectric Resonator Antenna Array Fed by Dielectric Image Guide," IEEE Transactions on Antennas and Propagation, Vol. 57, No. 8, pp. 2252-2259, 2009.

[14] A. S. Al-Zoubi, A. A. Kishk and A.W. Glisson "A Linear Rectangular Dielectric Resonator Antenna Array Fed by Dielectric Image Guide With Low Cross Polarization," IEEE Transactions on Antennas and Propagation, Vol. 58, No. 3, pp. 697-705, 2010.

[15] A. Rashidain, M. T. Aligodarz, L. Shafai and D. M. Klymyshyn, "On the Matching of Microstrip-Fed Dielectric Resonator Antennas," IEEE Transactions on Antennas and Propagation, Vol. 61, No.10, pp. 5291- 5296, 2013.

[16] L. Huitema, M. Koubeissi, M. Mouhamadou, Eric Arnaud, C. Decroze and T. Monediere, "Compact and Multiband Dielectric Resonator Antenna With Pattern Diversity for Multistandard Mobile Handheld Devices," IEEE Transactions on Antennas and Propagation, Vol. 59, No. 11, pp. 4201-4208, 2011.

[17] R. Tian, V. Plicanic, B. K. Lau and Z. Ying, "A Compact Six-Port Dielectric Resonator Antenna Array: MIMO Channel Measurements and Performance Analysis," IEEE Transactions on Antennas and Propagation, Vol. 58, No. 4, pp. 1369-1379, 2010.

[18] J. B. Yan and J. T. Bernhard, "Implementation of a Frequency-Agile MIMO Dielectric Resonator Antenna," IEEE Transactions on Antennas and Propagation, Vol. 61, No. 7, pp. 3434-3441, 2013.

[19] L.Z. Thamae and Z. Wu, "Dielectric resonator-based multiple-input multipleoutput antennas and channel characteristic analysis", *IET, Microwaves, Antennas and Propagation,* Vol. 6, No. 9, pp. 1084-1089, September 2012.

[20] Katsunori Ishimiya, Zhinong Ying and Jun-ichi Takada, "A Compact MIMO DRA for 802.11n application", *IEEE Intenrational Symposium on Antennas and Propagarion, (APS)*, CA, USA, 2008.

[21] M. S. Sharawi, S. K. Podilchak and Y. M. M. Antar, "A Low Profile Dual-Band DRA-Based MIMO Antenna System for Wireless Access Points", *IEEE Intenrational Symposium on Antennas and Propagarion, (APS)*, Vancouver, BC, Canada, 2015.

[22] Cisco Aironet Series 1700/2700/3700 access points, $www.cisco.com$.

[23] D-link DAP-2690 access point, $www.dlinkmea.com$

[24] A. Petosa, *Dielectric Resonator Antenna Handbook,* Artech House, 2007.

[25] K. M. Luk and K. W. Leung, *Dielectric Resonator Antennas*, Research Studies Press, 2003.

[26] S. Mikki and Y. M. M. Antar, "On Cross Correlation in Antenna Arrays With Applications to Spatial Diversity and MIMO Systems", *IEEE Transactions on Antennas and Propagation*, Vol. 63, No. 4, pp. 1798-1810, 2015.